

Classical density-functional theory of inhomogeneous water including explicit molecular structure and nonlinear dielectric response

Johannes Lischner and T.A. Arias

Laboratory of Atomic and Solid State Physics, Cornell University, Ithaca, New York 14853

(Dated: October 26, 2018)

We present an accurate free-energy functional for liquid water written in terms of a set of effective potential fields in which fictitious noninteracting water molecules move. The functional contains an *exact* expression of the entropy of noninteracting molecules and thus provides an ideal starting point for the inclusion of complex inter-molecular interactions which depend on the *orientation* of the interacting molecules. We show how an excess free-energy functional can be constructed to reproduce the following properties of water: the dielectric response; the experimental site-site correlation functions; the surface tension; the bulk modulus of the liquid and the variation of this modulus with pressure; the density of the liquid and the vapor phase; and liquid-vapor coexistence. As a demonstration, we present results for the application of this theory to the behavior of liquid water in a parallel plate capacitor. In particular, we make predictions for the dielectric response of water in the nonlinear regime, finding excellent agreement with known data.

PACS numbers: 71.15.Mb, 05.20.Jj, 77.84.Nh, 87.15.kr

INTRODUCTION

Water is the most important liquid on earth. Although its uniform phase already exhibits many fascinating properties and is currently an area of intensive research, the importance of the *inhomogeneous* phase in the chemical and biological sciences is even greater: as a solvent, water is ubiquitous in physical chemistry, biochemistry and electrochemistry. The associated phenomena include hydrophobic interactions [1, 2], protein folding [3, 4], the electrochemical interface [5], and phase transitions of confined liquids [6, 7]. Due to the complex interplay of hydrogen bonding, long-range polar interactions, and short-range excluded volume effects, developing a tractable theory to describe the solvent in the aforementioned systems remains a challenge [8].

Despite the importance, inherent interest, and extensive experimental study of water, most existing theories of the inhomogeneous phase of water either lack the accuracy to describe the above phenomena in a quantitatively satisfying way or become computationally prohibitive. The latter is particularly true for applications to complex systems, such as dissolved biomolecules or electrochemical interfaces. Simple dielectric continuum theories [9, 10] capture the dielectric response of the solvent at long length scales, but fail to describe more subtle effects at interfaces, such as the reorganization of the hydrogen-bond network or the binding of water molecules to solutes. Atomistic theories, on the other hand, describe such local effects quite well, but require the explicit treatment of many solvent molecules and also demand long simulation times to calculate statistically reliable thermodynamic averages. Since the full-fledged *ab initio* molecular dynamics description of the solvent is only feasible for the smallest solutes, generally additional approximations become necessary in practice: Bernholc

and coworkers, for example, have introduced a clever scheme which employs the full *ab initio* description only for a few solvent molecules adjacent to the solute and use rigid geometries and frozen electron densities for the remaining molecules [11]. In other studies, combination of *ab initio* methods for the solute with classical force field approaches [12, 13, 14] for the solvent yields additional simplifications. Despite the simplifications which such hybrid approaches allow, the need to compute many configurations to sample phase-space properly ultimately limits the size of systems which can be studied and thus the applicability of such approaches.

Ideally, one would have a rigorous description of the solvent which is able to combine the advantages of continuum theories (large system sizes and *implicit* thermodynamic averaging) with an explicit geometric description of the solvent molecule. Here, we show that just such a theory can be developed for liquid water by starting with the quantum mechanical free-energy functional for both the electrons and nuclei which comprise the liquid and, by “integrating out” the electrons, proceeding to construct a density functional in terms of atomic site densities alone. Such “classical” density-functional theories, which are founded on a number of exact theorems [15, 16], have been applied successfully to the study of simple liquids in the past [17, 18]. Historically, application of this method begins with a hard sphere reference system that is usually augmented by terms that capture weak long-range attractive forces [19]. Unfortunately, a hard sphere reference system is a poor starting point for the description of water because of the strong anisotropic short-range interactions arising from the molecular structure, including effects such as hydrogen bonding.

To remedy this, Chandler and coworkers [20, 21, 22] introduced a density-functional theory for general molecular liquids in terms of a set of densities, one for each

“interaction site” on the molecule (typically atomic centers). Although their theory successfully predicted the correct hydrogen-bonded structure of ice [22], it suffered from a significant flaw: to make calculations tractable, the “united atom approximation”, which takes all of the sites on the molecule to sit at a single point, had to be invoked. This severe oversimplification of the molecular structure prohibited the description of dielectric properties and stalled the further development of this promising approach. In [23], we eliminated the need for the united atom approximation by writing the free energy of a general molecular liquid as a functional of a set of effective potentials in which fictitious non-interacting molecules move. This advance allows for the exact evaluation of the entropy associated with the geometric structure of the molecules in a numerically feasible way and forms the basis for the construction of a new class of accurate density functionals for fully interacting *molecular* liquids.

In this work, we apply our general theory of molecular liquids to water and demonstrate how an accurate free-energy functional can be developed to reproduce the equation of state, the experimental site-site correlation functions, and the macroscopic dielectric response. The organization of the work is as follows. Section 2 gives a brief review of the general theory of molecular liquids introduced in [23]. Section 3 discusses the application of this approach to the particular case of water and introduces new computational techniques to simplify calculations of triatomic liquids. Section 4 presents results obtained using this new microscopically-informed continuum theory to study the behavior of water in a parallel plate capacitor. Here, we explore the differences between capacitor plates consisting either of purely repulsive hard walls or of walls with a local region of attraction. We also explore the dielectric response of water in both the linear and the nonlinear regimes of the applied field. Comparing our results to previous works based on explicit molecular simulations, we find quite encouraging agreement. Section 5 then concludes this work.

DENSITY-FUNCTIONAL THEORY OF MOLECULAR LIQUIDS

Kohn-Sham Approach and Entropy Functional

In [23], we showed that the grand free energy Ω of an assembly of interacting identical molecules (consisting of M atoms or “interaction sites” each) can be expressed as a functional of a set of effective potentials $\Psi = \{\Psi_1(\mathbf{r}), \dots, \Psi_M(\mathbf{r})\}$, in which a corresponding set of fictitious non-interacting molecules move. Specifically,

we wrote

$$\Omega[\Psi] = \Omega^{(ni)}[\Psi] - \sum_{\alpha=1}^M \int d^3r (\Psi_{\alpha}(\mathbf{r}) - \phi_{\alpha}(\mathbf{r}) + \mu_{\alpha}) n_{\alpha}(\mathbf{r}) + U[\mathbf{n}]. \quad (1)$$

Here, $\phi_{\alpha}(\mathbf{r})$ is the site-dependent external potential (with α referring to the different atomic sites on each molecule), μ_{α} is a site specific chemical potential and $U[\mathbf{n}]$ denotes the excess free energy due to inter-molecular interactions, which is a functional of the set of site densities $\mathbf{n} = \{n_1(\mathbf{r}), \dots, n_M(\mathbf{r})\}$. Finally, $\Omega^{(ni)}[\Psi]$ is the grand free energy of an assembly of noninteracting molecules in a set of effective potentials Ψ . This free energy is known explicitly and is *exactly*

$$\Omega^{(ni)}[\Psi] = -k_B T n_l \int d^3M r s(\{\mathbf{r}_{\alpha}\}) e^{-\beta \sum_{\alpha=1}^M \Psi_{\alpha}(\mathbf{r}_{\alpha})}, \quad (2)$$

where n_l is the reference density at vanishing chemical potentials (which we will later take to be the bulk liquid density) and $s(\{\mathbf{r}_{\alpha}\})$, which describes the geometry of the molecule, is the intra-molecular distribution function. Note that we take the densities in (1) to be themselves functionals of the effective fields via

$$n_{\alpha}(\mathbf{r}) = \frac{\delta \Omega^{(ni)}}{\delta \Psi_{\alpha}(\mathbf{r})}[\Psi]. \quad (3)$$

Finally, the effective potentials which minimize $\Omega[\Psi]$ determine the equilibrium site densities and allow for the calculation of various equilibrium properties of the liquid.

The introduction of effective potentials instead of site density fields as fundamental variables in the density-functional theory of classical molecular liquids allows for the first time a computationally tractable approach to treat the non-interacting system exactly. This parallels the introduction of Kohn-Sham orbitals as fundamental variables in the density-functional theory of electronic structure [24]. In both cases, the construction of highly accurate density functionals is made possible by mapping a system of interacting particles onto a fictitious system of noninteracting particles with the same equilibrium densities. We mention that our approach of minimizing the free energy with respect to a set of *effective potentials* is known in the electronic structure context as the optimized effective potential method [25].

Excess Free Energy Functional

In [23], we also present a recipe for the construction of the excess free energy functional U in (1). As usual with density-functional theories, this construction is difficult. As in our previous work, we follow the lead of Kohn and Sham and construct a free-energy functional that reproduces established results for the homogeneous phase in

the limit of vanishing external fields. Namely, we expand U in a power series about the uniform liquid, and formally group all terms except the quadratic part, which is analogous to the Hartree energy in electronic-structure theory, into an unknown functional $F^{ex}[\mathbf{n}]$, which is then the analogue to the electronic exchange-correlation functional, whose form, being unknown, must ultimately be treated in some approximate way.

To proceed, we separate the kernel of the quadratic part of U into a long-wavelength part $K_{\alpha\gamma}$, known analytically for the case of rigid molecules, and a remainder $C_{\alpha\gamma}$, to be determined from experimental data. The next paragraph describes $K_{\alpha\gamma}$ in detail, and the set of functions $C_{\alpha\gamma}$ will be constructed below such that the resulting functional reproduces the experimental correlation functions in the uniform phase. When these two parts are determined, they combine with F^{ex} to give U as

$$U[\mathbf{n}] = \frac{1}{2} \sum_{\alpha,\gamma=1}^M \int d^3r \int d^3r' n_{\alpha}(\mathbf{r}) \{K_{\alpha\gamma}(\mathbf{r}, \mathbf{r}') + C_{\alpha\gamma}(\mathbf{r}, \mathbf{r}')\} n_{\gamma}(\mathbf{r}') + F^{ex}[\mathbf{n}]. \quad (4)$$

The derivation of $K_{\alpha\gamma}$ [23] considers a collection of rigid neutral molecules with each interaction site carrying a partial charge q_{α} with *no* assumptions regarding the form of the non-electrostatic part of the interaction — the theory neither is perturbative in the interaction strength nor presupposes a decomposition into pairwise interaction potentials. In [23], we then prove rigorously that, for a certain class of liquids including all diatomic liquids and also water, the leading order term in a long-wavelength expansion of $\partial_{\mathbf{n}}^2 U$, the Hessian of U for rigid molecules, is

$$K_{\alpha\gamma}(\mathbf{k}) = \left(\frac{\epsilon}{\epsilon - 1} - \frac{\epsilon^{(ni)}}{\epsilon^{(ni)} - 1} \right) \frac{4\pi}{\mathbf{k}^2} q_{\alpha} q_{\gamma}, \quad (5)$$

where ϵ is the macroscopic dielectric constant and $\epsilon^{(ni)}$ is the dielectric constant of a system with intra-molecular correlations only. Because $K_{\alpha\gamma}$ now captures the singular long-wavelength features of the response function, $C_{\alpha\gamma}$, which we define as the difference between $\partial_{\mathbf{n}}^2 U$ (given by the experimental correlation functions) and the sum of $K_{\alpha\gamma}$ and $\partial_{\mathbf{n}}^2 F^{ex}$, must now be smooth near the origin and thus amenable to numerical approximations. As discussed below, we define F^{ex} such that its Hessian matches the constant term in the long-wavelength expansion of $\partial_{\mathbf{n}}^2 U$. Therefore, the functions $C_{\alpha\gamma}$ have to *vanish* for small \mathbf{k} .

Next, to approximate F^{ex} , we begin by noting that in the case of zero external fields all densities are equal and the first quadratic term (K) in (4) vanishes because of charge neutrality. Anticipating that, by definition, the matrix function C vanishes in the long-wavelength limit,

F^{ex} then captures all of the internal energy of the uniform phase (and the long-wavelength limit of the non-singular part of the Hessian $\partial_{\mathbf{n}}^2 U$) and can be expressed as $F^{ex} = V f^{ex}(n)$, with V being the volume and n the average molecular density. Due to the presence of multiple density fields, generalizing the above expression for F^{ex} to the inhomogeneous case is more difficult than for the analogous exchange-correlation energy in electronic structure theory. Moreover, because of the strong correlations induced by excluded volume effects, *purely local* excess functionals fail to describe the liquid state [26]. We therefore approximate F^{ex} with a simplified *ansatz* in the spirit of weighted density-functional theory [26], but generalized to multiple species,

$$F^{ex}[\mathbf{n}] = \int d^3r \sum_i p_i f^{ex} \left(\sum_{\gamma=1}^M b_{\gamma}^i \bar{n}_{\gamma}(\mathbf{r}) \right), \quad (6)$$

where we introduce the weighted densities $\bar{n}_{\gamma}(\mathbf{r}) = \int d^3r' (\pi r_0^2)^{-3/2} \exp(-|\mathbf{r} - \mathbf{r}'|^2/r_0^2) n_{\gamma}(\mathbf{r}')$, with r_0 being a “smoothing” parameter ultimately fit to the experimental surface tension. To reduce to the correct form in the uniform case, p_i and b_{γ}^i must fulfill $\sum_i p_i = 1$ and $\sum_{\gamma=1}^M b_{\gamma}^i = 1$.

For the scalar function $f^{ex}(n)$, we use a polynomial fit to various bulk thermodynamic properties of the liquid. The condition that C vanishes in the long-wavelength limit subsequently fixes p_i and b_{γ}^i . For a given r_0 , this then completely specifies our approximation to F^{ex} . Next, relating $K + C + \partial^2 F^{ex}$ to the density-density correlation functions through the Ornstein-Zernike relation gives the matrix function C for a given r_0 . Finally, we can determine the smoothing parameter r_0 by adjustment until calculations of the liquid-vapor interface give the correct surface tension.

APPLICATION TO WATER

Intra-molecular Free Energy

Assuming rigid bonds of fixed length (and thus rigid angles as well) the intra-molecular distribution function of a water molecule (normalized to integrate to the volume of the system) is

$$s(\mathbf{r}_0, \mathbf{r}_1, \mathbf{r}_2) = \frac{\delta(|\mathbf{r}_{10}| - B)}{4\pi B^2} \frac{\delta(|\mathbf{r}_{20}| - B)}{4\pi B^2} \times 2\delta(\hat{\mathbf{r}}_{10} \cdot \hat{\mathbf{r}}_{20} - \cos \theta_B), \quad (7)$$

where $B = 1 \text{ \AA}$ is the oxygen-hydrogen bond length taken from the SPC/E [27] model of water, θ_B is the bond angle between the hydrogens and taken to be the tetrahedral angle like in the SPC/E model. Also, the label 0 refers to the oxygen atom and the labels 1 and 2 to the two hydrogens, and we define $\mathbf{r}_{ij} \equiv \mathbf{r}_i - \mathbf{r}_j$. Contrary to

the case of diatomic molecules, where the assumption of rigid bonds turns $\Omega^{(ni)}$ into a convolution, numerical evaluation of (2) proves more challenging in the triatomic case because of the complex, nine-dimensional form of s .

To address this, we observe here that $\Omega^{(ni)}$ for water can *also* be brought into a “convolution form” by making use of the following mathematical identity, which is readily derived using the addition theorem for spherical harmonics,

$$\delta(\hat{\mathbf{v}} \cdot \hat{\mathbf{w}} - \cos \zeta) = \sum_{lm} 2\pi P_l(\cos \zeta) Y_{lm}^*(\hat{\mathbf{v}}) Y_{lm}(\hat{\mathbf{w}}), \quad (8)$$

where $\hat{\mathbf{v}}$ and $\hat{\mathbf{w}}$ are unit vectors, ζ is an arbitrary angle, P_l is a Legendre polynomial and the Y_{lm} ’s denote the spherical harmonics. (To prove (8), first expand the delta function as a sum of pairs of Legendre polynomials on the interval $[-1; 1]$ and then use the spherical-harmonic “addition theorem” to express $P_l(\hat{\mathbf{v}} \cdot \hat{\mathbf{w}})$ as a sum of pairs of spherical harmonics.)

Substituting (8) and (7) into (2) results in a computationally efficient form for the non-interacting free energy $\Omega^{(ni)}$,

$$\begin{aligned} \Omega^{(ni)} &= -k_B T n_l \int d^3 r_0 e^{-\beta \Psi_0(\mathbf{r}_0)} \\ &\times \sum_{lm} 4\pi P_l(\cos \theta_B) f_{lm}^{(1)}(\mathbf{r}_0) f_{lm}^{(2)}(\mathbf{r}_0), \end{aligned} \quad (9)$$

where $f_{lm}^{(1)}$ and $f_{lm}^{(2)}$, given by

$$\begin{aligned} f_{lm}^{(1)}(\mathbf{r}_0) &= \int d^3 r_1 \frac{\delta(|\mathbf{r}_1 - \mathbf{r}_0| - B)}{4\pi B^2} Y_{lm}^*(\hat{\mathbf{r}}_{10}) e^{-\beta \Psi_1(\mathbf{r}_1)} \\ f_{lm}^{(2)}(\mathbf{r}_0) &= \int d^3 r_2 \frac{\delta(|\mathbf{r}_2 - \mathbf{r}_0| - B)}{4\pi B^2} Y_{lm}(\hat{\mathbf{r}}_{20}) e^{-\beta \Psi_2(\mathbf{r}_2)} \end{aligned} \quad (10)$$

are now convolutions and can be efficiently evaluated with fast-Fourier-transform techniques. Transformation to Fourier space greatly simplifies the above convolutions,

$$\begin{aligned} f_{lm}^{(1)}(\mathbf{k}) &= (-i)^l j_l(|\mathbf{k}|B) Y_{lm}^*(\hat{\mathbf{k}}) \mathcal{F}[e^{-\beta \Psi_1(\mathbf{r})}] \\ f_{lm}^{(2)}(\mathbf{k}) &= (-i)^l j_l(|\mathbf{k}|B) Y_{lm}(\hat{\mathbf{k}}) \mathcal{F}[e^{-\beta \Psi_2(\mathbf{r})}], \end{aligned} \quad (11)$$

where j_l denotes the spherical Bessel functions of the first kind and $\mathcal{F}[\exp(-\beta \Psi_1(\mathbf{r}))]$ denotes the Fourier transform of $\exp(-\beta \Psi_1(\mathbf{r}))$.

To evaluate (9) numerically, we first choose a maximum value of l , l_{max} , after which we truncate the infinite sum. In general, the choice of l_{max} depends on the density profile that has to be represented. We find in the capacitor calculation presented below that the interaction site densities for water adjacent to the capacitor wall are fairly smooth in the linear response regime and can be sufficiently resolved with $l_{max} = 10$. If strong external fields are applied, sharp features in the density profile develop and we use $l_{max} = 40$ to be absolutely sure of a highly converged description.

ρ_l [kg/m ³]	ρ_v [kg/m ³]	B_l [GPa]	$\partial B_l / \partial P$ (dimensionless)
997.1	0.023	2.187	5.8

TABLE I: Experimental inputs to construction of f^{ex} from [28] and [29]: liquid density (ρ_l), vapor density (ρ_v), liquid bulk modulus (B_l) and derivative of modulus with respect to pressure ($\partial B_l / \partial P$).

f_0	[hartree \times bohr ⁻³]	3.7608 5540 7008 46 $\times 10^{-18}$
f_1	[hartree]	-9.9058 0951 0335 88 $\times 10^{-11}$
f_2	[hartree \times bohr ³]	8.6971 6797 7040 56 $\times 10^{-4}$
f_3	[hartree \times bohr ⁶]	-2.5454 6838 7756 12 $\times 10^3$
f_4	[hartree \times bohr ⁹]	8.9610 5939 0318 49 $\times 10^5$
f_5	[hartree \times bohr ¹²]	-1.2391 1957 0697 09 $\times 10^8$
f_6	[hartree \times bohr ¹⁵]	6.4173 3045 2123 21 $\times 10^9$

TABLE II: Coefficients of polynomial parametrization of f^{ex} given to all digits used in our software in order to ensure numerical reproducibility of our results. Any individual coefficient contains at most two or three significant figures.

Intermolecular Free Energy

First, we approximate $f^{ex}(n)$ as a sixth-order polynomial,

$$f^{ex}(n) = \sum_{p=0}^6 f_p n^p, \quad (12)$$

and adjust its coefficients to reproduce the seven conditions represented by (a) the thermodynamic stability of liquid and vapor phases, (b) their coexistence, (c) the experimental liquid and vapor densities, (d) the experimental bulk modulus of the liquid (B_l) and (e) the derivative of the bulk modulus with respect to the pressure P at standard temperature and pressure ($T = 25$ °C and $P = 101.325$ kPa $\equiv 1$ atm). Table I summarizes the experimental input used to determine the coefficients f_p , and Table II gives the actual numerical values of the coefficients used in our calculations below. (Clearly, not all of the digits given in the table are significant, we give them only to make our results numerically reproducible.) The values in the table are given in atomic units (1 hartree ≈ 27.21 eV, 1 bohr ≈ 0.5291 Å) as this is the system which our software employs.

Next, we can determine the coefficients in the integrand in (6) from knowledge of the constant term in the long-wavelength expansion of the Hessian $\partial_{\mathbf{n}}^2 U$. The entries in this term (which is a matrix) are related to various material response properties such as as the bulk modulus, but unfortunately, we do not have access to data for all of the material properties. In the absence of data, we take this matrix to be proportional to its value for the

non-interacting case with a proportionality constant set to ensure the correct bulk modulus. This then fixes the integrand in (6) and allows it to be written entirely in terms of rational numbers in the form,

$$-\frac{19}{20}f^{ex}(\bar{n}_0) + \frac{3}{10}f^{ex}(\bar{n}_1) + \frac{3}{10}f^{ex}(\bar{n}_2) + \frac{27}{20}f^{ex}\left(\frac{\bar{n}_0 + \bar{n}_1 + \bar{n}_2}{3}\right). \quad (13)$$

Next, to construct the matrix K we use the partial charges of the SPC/E water model [27], i.e. $q_1 = q_2 = -q_0/2 = 0.4238e$ (e being the proton charge) and the fact that the dielectric constant of the liquid with intramolecular correlations *only* is $\epsilon^{(ni)} = (1 - 4\pi\beta n_i p^2/3)^{-1}$, where p is the dipole moment of an SPC/E water molecule. Also, we employ the experimental value [28], $\epsilon = 78.4$, for the macroscopic dielectric function of liquid water at standard conditions described above.

The use of K as leading order term is only justified for *long-wavelength* (small \mathbf{k}) properties of the liquid: we therefore cut off its slowly decaying, large \mathbf{k} tail by multiplying it in Fourier space with a crossover function λ_{cr} given by

$$\lambda_{cr}(\mathbf{k}) = \frac{1}{(1 + |\mathbf{k}|/k_c)^4}, \quad (14)$$

with $k_c = 0.33$ bohr, chosen to keep the C functions as band-width limited as possible.

Then we determine C as described above using the partial structure factor data for the uniform liquid from Figure 1 in [30]. The best, explicit partial structure factor data which we have found are measured at standard pressure, but at a temperature $T = 20 \pm 3$ °C, which differs slightly from the standard temperature ($T = 25$ °C) employed in this work. Comparing experimental radial distribution functions at various temperatures [31], we find that the differences remain smaller than 10% over a temperature range of 30 Kelvin. We therefore expect an overall error of no more than one or two percent due to this difference in temperatures. Next, adjusting the smoothing parameter to give the experimental surface tension of 71.98×10^{-5} N/m[28], measured at standard conditions, yields $r_0 = 4.2027$ bohr (to all the digits used in our software). Finally, to provide a computationally transferable representation of C , we parametrize each component $C_{\alpha\gamma}$ by a sum of Gaussians in Fourier space

$$C_{\alpha\gamma}(\mathbf{k}) = \sum_{i=1}^{N_{\alpha\gamma}} A_{\alpha\gamma}^{(i)} \exp\left\{-B_{\alpha\gamma}^{(i)}\left(|\mathbf{k}| - C_{\alpha\gamma}^{(i)}\right)^2\right\}. \quad (15)$$

Table III summarizes the resulting fitting coefficients (to all decimal places used in our software). To reproduce the full matrix, note that C is symmetric and that the identity of the hydrogens imposes $C_{11} = C_{22}$. Figure 1

	i	$A_{\alpha\gamma}^{(i)}$ [hartree]	$B_{\alpha\gamma}^{(i)}$ [bohr ²]	$C_{\alpha\gamma}^{(i)}$ [bohr ⁻¹]
C_{00}	1	-0.0271 1530	1.0569 0000	0.0204 8180
	2	-0.0795 5700	1.6385 3000	0.1295 1300
	3	0.0966 4800	1.8781 5000	0.0736 7760
	4	-0.0291 5170	2.4678 7000	0.0563 6360
	5	0.0227 0520	3.1004 7000	0.0844 1320
	6	-0.0109 0780	3.7162 0000	0.0452 0230
C_{01}	1	-0.0080 1259	1.1985 9000	0.0280 2800
	2	0.0379 8360	1.7289 7000	0.1175 3400
	3	-0.0380 7370	2.1583 9000	0.2133 3600
	4	0.0254 5760	2.7211 2000	0.1541 5700
	5	-0.0029 1329	3.2989 4000	0.0265 2820
	6	0.0010 9967	3.7659 0000	0.0315 5180
C_{11}	1	-0.0139 5900	1.8869 7000	0.1041 8600
	2	0.0295 7760	2.5316 4000	0.0869 8480
C_{12}	1	-0.0139 5900	1.8869 7000	0.1041 8600
	2	0.0295 7760	2.5316 4000	0.0869 8480

TABLE III: Coefficients of Gaussian parametrized C functions. Note that, by symmetry, $C_{\alpha\gamma} = C_{\gamma\alpha}$ and $C_{11} = C_{22}$. (C_{12} and C_{11} turned out to be numerically indistinguishable.) Coefficients are given to all digits used in our software to ensure numerical reproducibility of our results. The index 0 refers to the oxygen site, the indices 1 and 2 refer to the two hydrogen sites.

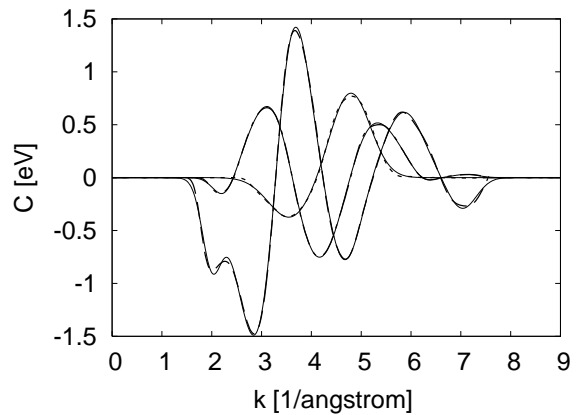


FIG. 1: Comparison of C_{00} (thick dashed curve), C_{01} (thick dash-dotted curve) and C_{11} (thick dotted curve) and the corresponding parametrized forms (thin solid curves) given by (15) and Table III. Note that C_{12} is not shown, since it would be visually indistinguishable from C_{11} .

compares our extracted C functions to the resulting numerical fits, the latter of which are used in all of the calculations presented below.

Recipe for Evaluating the Free Energy Functional for Water

In sum, to compute the free-energy functional for a given set of effective potentials $\Psi_\alpha(\mathbf{r})$, one first evaluates the intra-molecular contribution via (9) and (11). Next, one determines the site densities via (3), which allows one to evaluate the second term in (1) trivially. Finally, one evaluates the last term in (1) according to (4), with K given by (5), C parameterized by the coefficients in Table III, and F^{ex} computed according to (6), (12), (13).

WATER IN A PARALLEL PLATE CAPACITOR

To demonstrate the ability of our density-functional theory to describe water in an inhomogeneous environment and to capture the dielectric response of the liquid, we study the behavior of the liquid in a parallel plate capacitor. We carry out our study at standard temperature and pressure described above, taking the system to be homogeneous in the two dimensions parallel to the capacitor plates. Along the perpendicular direction, we impose periodic boundary conditions, defining a unit cell containing *two* parallel plate capacitors with opposing externally applied electric fields. This arrangement makes the electrostatic potential a periodic function and eliminates undesired electrostatic interactions between the capacitors. Each capacitor has a plate separation of 106 Å (200 bohr) and the total length of the cell is 423 Å (800 bohr).

In our study we consider both purely repulsive, “hard-wall” plates as well as “attractive” plates with a region of attraction near the plates. For the hard-wall case, the plates are essentially infinite potential hard walls acting on both the oxygen and hydrogen sites of the water molecules. As a practical numerical matter, to reduce aliasing effects in the use of the numerical Fourier transform we approximate such walls by purely repulsive Gaussian potentials of sufficiently narrow width and large amplitude so that the results below are insensitive to the width and amplitude of the Gaussian employed. In particular, we use

$$\phi_{hw}(z) = A \exp\left(-\frac{z^2}{2a^2}\right), \quad (16)$$

with $A = 150 k_B T$ and $a = 0.5 \text{ \AA}$. For the attractive case, we employ a “9-3” (planarly integrated Lennard-Jones) potential acting on the oxygens *only*, specifically,

$$\phi_{at}(z) = C \left[\left(\frac{D}{z + z_{\text{shift}}} \right)^9 - \left(\frac{D}{z + z_{\text{shift}}} \right)^3 \right] \quad (17)$$

with $C = 9 \times 0.15 / (2\sqrt{3}) \text{ eV}$, $D = \frac{5}{3176} \text{ \AA}$ and $z_{\text{shift}} = 2 \text{ \AA}$. This potential has its minimum at a distance of 3 Å from the wall at a depth 0.15 eV. We choose this depth as

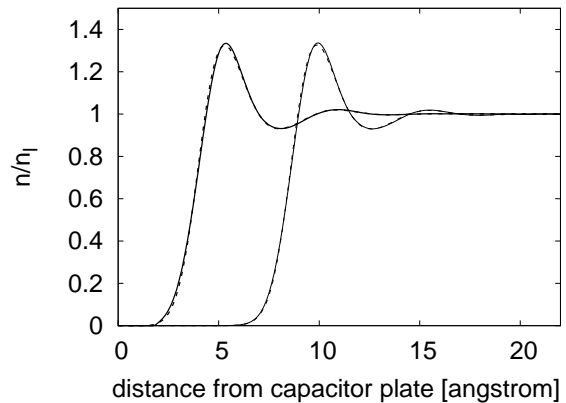


FIG. 2: Hydrogen- (thick dotted curve) and oxygen- (thick solid curve) site density in weak field and zero field (thin curves) versus distance from hard-wall plate. (Note that the hydrogen and oxygen densities are nearly visually indistinguishable.)

typical of the interactions in such systems. For instance, Berkowitz and co-workers [32] employ a corrugated potential with an average depth of about 0.40 eV, which is also in the range of a couple of tenths of an electron Volt.

To determine the thermodynamic state of the system we then expand the density fields on a real space grid with 8192 sampling points (~ 20 points/Å), and minimize the grand free energy (1) using standard numerical conjugate gradient techniques without any preconditioning.

Results

Hard-wall plates

We begin with a brief discussion of our results for the hard wall case as an idealized reference for comparison. Figure 2 shows our results for oxygen and hydrogen equilibrium density profiles in the absence of an externally applied electrostatic displacement ($D = 0$) and compares them to the density profiles of hydrogen and oxygen sites in a relatively weak external field ($\alpha \equiv \beta p D / \epsilon \approx 0.009$). The zero-field profiles exhibit an extended gas phase region up to a distance of $\sim 10 \text{ \AA}$ from the plates. This “lingering” gas phase region exists because molecules can, at very little free-energy cost, minimize the influence of the repulsive plates by leaving the system. (Recall that (1) is written in the grand canonical ensemble, so that the system can exchange particles with an external reservoir.) As soon as a relatively weak external electric displacement is applied, however, it becomes favorable for the dipolar molecules to enter the system because they can lower their energy by partially aligning with the field within the capacitor. For even quite small fields, this effect causes the capacitor to fill with liquid, thereby elim-

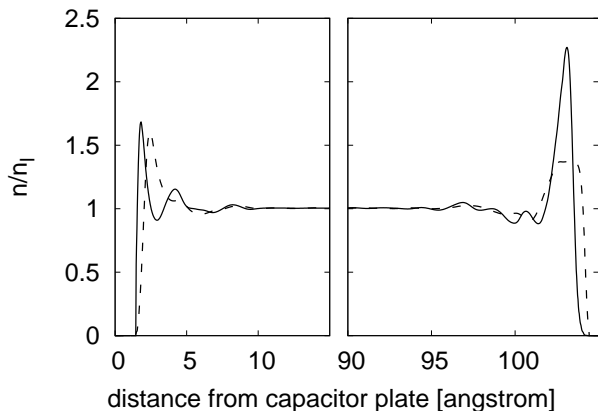


FIG. 3: Hydrogen- (dashed curve) and oxygen- (solid curve) site density in strong field versus distance from hard-wall plate.

inating most of the gas phase region. The result of this is then an almost rigid shift of the density profiles toward the capacitor plates, with an appearance and general shape which remains nearly fixed over a large range of fields.

Considering the fine details of the density profiles, we note that, contrary to our previous results for diatomic liquids, a relatively small (barely noticeable in the figure) asymmetry exists at zero external field between the oxygen and hydrogen site densities so that there is a non-vanishing electrostatic charge density in the vicinity of the capacitor plates — even in the absence of an externally applied electric field. (Note: because the oxygen site carries a charge which is double in magnitude compared to the hydrogen site and because there are two independent but identical hydrogen sites, the magnitude of the charges carried by the oxygen and hydrogen density fields are directly proportional to the curves in the figure, *with the same constant of proportionality* for each.) By symmetry, the net charge which the plates induce must integrate to zero; however, a finite surface dipole remains with a corresponding potential jump which we find in the zero-field hard-wall case to be +0.041 V across the solid-liquid interface, with the potential being higher in the solid.

Figure 3 shows the equilibrium density profiles in a relatively strong ($\alpha \approx 0.25$) external field directed from left to right in the figure. The relative abundance of oxygen sites close to the left plate (which carries a positive external charge to generate the field) and of hydrogen sites next to the right plate (which carries a negative external charge) indicates that the water molecules exhibit a strong tendency to align their dipoles with the applied field. Interestingly, this leads to quite different density profiles on the opposite sides of the capacitor. On the left (positive) plate, the first peak in the oxygen density is followed by a peak in the hydrogen density of similar

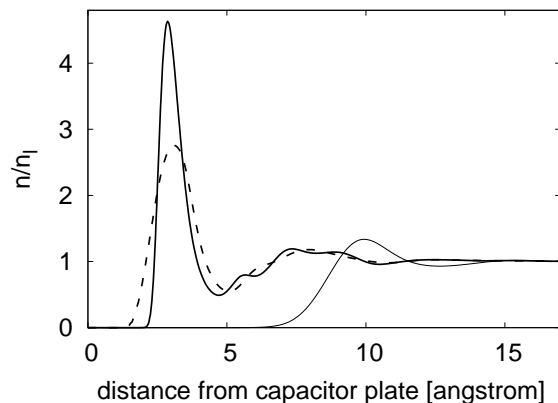


FIG. 4: Hydrogen- (thick dashed curve) and oxygen- (thick solid curve) site density in strong field versus distance from attractive wall. Reference result for the zero field oxygen density at repulsive wall (thin solid curve).

shape, width and height. This we interpret to be a direct consequence of alignment of the molecules with the field and the rigid intra-molecular bonding between hydrogen and oxygen atoms, an effect quite similar to what was observed in our previous study of liquid hydrogen chloride[23]. The distance between these peaks, 0.65 Å, is within about 10% of 0.58 Å, what one expects from the basic geometry of the water molecule assuming that the molecules fully align with the field.

On the right (negative) plate, we again find a well-defined peak in the oxygen density, though the peak is somewhat stronger than on the left. We find also that the hydrogen density, rather than being also sharply peaked, is now spread significantly around the oxygen peak. This case is different, because the hydrogen sites, now pointing away from the liquid region, cannot form hydrogen bonds if the molecules align fully with the field.

Attractive plates

Figure 4 compares the zero-field results for the hard-wall plates with those of the attractive plates. There is no longer a “lingering” gas phase region because the minimum in the interaction potential (acting only on the oxygen sites in this case) with the plates sets the location of the main peak in the oxygen density. This minimum, as described above, occurs at a distance of about 3 Å from the attractive walls and corresponds well with the peaks in the oxygen and hydrogen density profiles. The height of the oxygen peak is larger than the density in the bulk by a factor of ~ 4.7 , which is similar to the results of molecular dynamics calculations of water adjacent to platinum surfaces [32] and experimental findings [33]. Finally, there is also a net dipole layer in our attractive case leading now to a significantly stronger

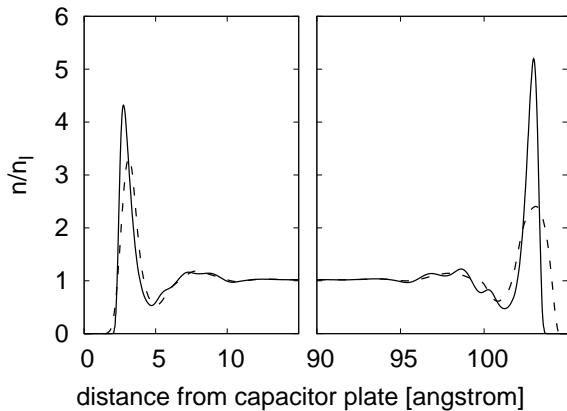


FIG. 5: Hydrogen- (dashed curve) and oxygen- (solid curve) site density in strong field versus distance from attractive wall.

potential jump at the liquid-solid interface of $+0.220$ V, with the potential in the solid again being higher. This value is typical of realistic systems: from molecular dynamics data of water adjacent to a platinum surface[34], we extract a potential jump of $\sim +0.5$ V with the potential being higher in the solid.

When a strong field (again, $\alpha \approx 0.25$) is applied to the capacitor with attractive walls (Figure 5), we find a rearrangement of the liquid structure which exhibits various quantitative differences compared to the hard-wall case: the oxygen peaks are now significantly more pronounced (reaching values near 4 and 5 times the equilibrium liquid density, as opposed to the previous peak values near 1.5 and 2.2) as the oxygen atoms settle into the attractive potential wells near the walls. Also, the peak near the positive plate is also now notably broader (with a width of 1.6 Å at the value of the equilibrium, as opposed to the previous value of 1.0 Å). Finally, the hydrogen peak is significantly less pronounced relative to the oxygen peak and the peak position is now less displaced (0.4 Å) from the oxygen peak position. Despite these quantitative differences, however, the qualitative features at strong fields are quite similar in the attractive and the hard-wall cases. Namely, on the left (positive) plate we find a well-defined peak in the oxygen density followed by a corresponding peak in the hydrogen density, and on the right (negative) plate there is a well-defined oxygen peak which is surrounded by a more diffuse peak in the hydrogen density. Also, as with the hard wall case, we find that the hydrogen peak is off-center from the oxygen peak and displaced toward the negative plate to which it is attracted.

This suggests that, at these large field strengths, general features are independent of the exact form of the liquid-solid interaction. In fact, we note that this sort of asymmetry between positive and negative plates is also evident in molecular dynamics calculations which, at fields near $\alpha = 0.25$, also tend to show that, near the positive plate, the oxygen density exhibits peaks which

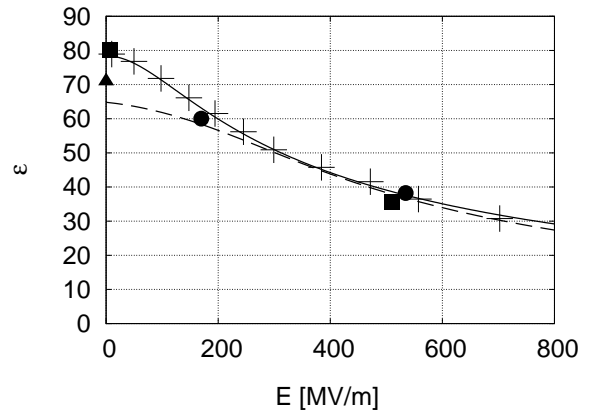


FIG. 6: Dielectric function versus total field: density-functional results (crosses), non-linear electrostatics (solid curve), analytical result of [36](dashed line), molecular dynamics results of [34](circles), [37](squares) and [38](triangles).

are followed by peaks of similar appearance in the hydrogen density, whereas, near the negative plate, there is a well-defined peak in the oxygen density but that the hydrogen density exhibits either a broader peak or multiple sub-peaks in the vicinity of the main oxygen peak[34, 35].

Nonlinear dielectric response

The equilibrium site densities also determine the dielectric function of water $\epsilon(D) = D/E(D)$ with E being the total electric field given by the sum of the electric displacement and the induced electric field. Although E has a complicated form close to the walls, it rapidly approaches the constant value $E = D - 4\pi P$ as the distance from the walls increases, where P is the induced polarization. In the present one-dimensional geometry, P is proportional to the induced surface charge which appears in the equilibrium density profiles.

Figure 6 shows our calculated results for ϵ plotted as a function of E in units of MV/m (equivalent to 1 mV/nm or 0.1 mV/Å) to simplify comparison with the results of previous studies. The figure shows that the results from our density-functional theory are well-described by self-consistently screened nonlinear electrostatics (solid curve), which gives the polarization P as the self-consistent solution to the equation $P = P^{(ni)}(D - a_\epsilon 4\pi P)$, where $P^{(ni)}(E)$ is the response of a gas of noninteracting dipoles in a local field E and $a_\epsilon \equiv \epsilon/(\epsilon - 1) - \epsilon^{(ni)}/(\epsilon^{(ni)} - 1)$ ensures that the correct linear response is recovered when D is weak. The solid curve reproduces our data well and so represents a convenient analytic guide to the eye for our results.

Figure 6 compares our results to Booth's analytical re-

sult for the nonlinear dielectric response of water [36]. This result (dashed curve in the figure) was obtained by extending Onsager's and Kirkwood's theories of polar dielectrics to high field strengths [36] and also reproduces quite well explicit molecular dynamics results for high fields. It fails, however, at small fields, eventually giving an incorrect linear dielectric constant of about ~ 65 . We find very good agreement with this established result for fields larger than 300 MV/m. We also compare our results to various molecular dynamics calculations [34, 37, 38] and find very good agreement, except at zero field, where the results of the molecular dynamics calculations often show a wide range of results, some differing significantly from the experimental dielectric constant of ~ 80 depending on the model potentials and numerical methods employed[39]. The zero-field dielectric constant, we, of course, reproduce exactly by construction. Our results, therefore, appear to be reliable over a broad range of applied fields.

SUMMARY AND CONCLUSIONS

This work demonstrates how to apply a new, general Kohn-Sham classical density-functional approach for molecular liquids to what is arguably the liquid of greatest scientific interest, water. The resulting theory has the quite tractable computational cost of the problem of a noninteracting gas of molecules in a self-consistent external potential and gives an exact account of the entropy associated with the alignment of the molecular dipole moment with an external field.

After constructing the functional and giving a complete numerical parameterization of all quantities so that our results are numerically reproducible, we demonstrate the tractability of the approach by applying it to the behavior of water in parallel plate capacitors, with either hard-wall or attractive plates, over a range of applied fields through which the dielectric constant ϵ of water varies by over a factor of two. We provide results for the distribution of oxygen and hydrogen atoms near the capacitor plates and find an asymmetry between the response at negatively and positively charged plates in general qualitative agreement with molecular dynamics results. From the resulting charge distributions, we extract predictions of the dielectric constant of water over a wide range of field strengths (0 to 800 MV/m) and find results in very good agreement with both previous theoretical and molecular dynamics calculations. The aforementioned exact treatment of the entropy cost of aligning the molecules with the field is critical in producing this accurate treatment of dielectric saturation effects.

With a successful framework in place, there is now a firm basis for future improvements. Given that we now have a good treatment of the internal structure of the water molecule, the primary area remaining for im-

provement is our choice to employ for this first work a somewhat simplistic weighted-density functional form in (6). The direct route to improve upon this is to leverage much of the existent work in simple fluids, both in traditional weighted density-functional theories[26] and in fundamental measure theory[40]. Another clear area for improvement would be the inclusion of additional, ionic species into the functional to allow for screening by electrolytes, which should be relatively straightforward.

In sum, we present a new framework for a computationally tractable continuum description of water which captures, within a unified approach with a firm theoretical foundation, molecular-scale correlations, entropic effects, microscopic dielectric screening, surface tension, bulk thermodynamic properties, and dielectric saturation. This description thus includes *a priori* all of the various effects which are generally added *a posteriori* to continuum models of water. Although less detailed than current explicit molecular treatments of the solvent, freed from the need for computing thermodynamic averages, a sufficiently accurate continuum approach such as we present has the potential to open up much larger and complex systems to theoretical study. As such, the new framework is an ideal starting point for a variety of new investigations into a wide class of subjects, which include protein folding, molecular motors, membrane physics, drug design, the electrochemical interface, liquid-phase catalysis and fuel cells.

ACKNOWLEDGEMENTS

T.A.A. was supported in part by NSF Grant No. CHE-0113670, and J.L. acknowledges support by DOE Grant No. DE-FG02-07ER46432.

-
- [1] D. Chandler, *Nature* **437**, 640 (2005).
 - [2] H. Ashbaugh and L. Pratt, *Rev. Mod. Phys.* **78**, 159 (2006).
 - [3] P. Liu, X. Huang, R. Zhou, and B. Berne, *Nature* **437**, 159 (2005).
 - [4] M. Tarek and D. Tobias, *Phys. Rev. Lett.* **88**, 138101 (2002).
 - [5] T. Tansel and O. Magnussen, *Phys. Rev. Lett.* **96** (2006).
 - [6] G. Hummer, J. Rasaiah, and J. Noworyta, *Nature* **414**, 188 (2001).
 - [7] Y. Leng and P. Cummings, *Phys. Rev. Lett.* **94**, 026101 (2005).
 - [8] J.-P. Hansen and I. McDonald, *Theory of Simple Liquids* (Academic Press, London, 2006).
 - [9] S. Miertus, E. Scrocco, and J. Tomasi, *Chem. Phys.* **55** (1981).
 - [10] R. Cammi and J. Tomasi, *J. Comput. Chem.* **16** (1995).
 - [11] M. Hodac, W. Lu, and J. Bernholc, *J. Chem. Phys.* **128** (2008).
 - [12] A. Warshel and M. Levitt, *J. Mol. Biol.* **102** (1976).

- [13] U. Singh and P. Kollmann, *J. Comput. Chem.* **7** (1986).
- [14] M. Field, P. Bash, and M. Karplus, *J. Comput. Chem.* **11** (1990).
- [15] N. Mermin, *Phys. Rev.* **137**, A1441 (1965).
- [16] N. Ashcroft, *Aust. J. Phys.* **49**, 3 (1996).
- [17] C. Ebner, W. Saam, and D. Stroud, *Phys. Rev. A* **14**, 2264 (1976).
- [18] W. Curtin and N. Ashcroft, *Phys. Rev. Lett.* **56**, 2775 (1986).
- [19] J. Weeks, K. Katsov, and K. Vollmayr, *Phys. Rev. Lett.* **81**, 4400 (1998).
- [20] D. Chandler, J. McCoy, and S. Singer, *J. Chem. Phys.* **85**, 5971 (1986).
- [21] D. Chandler, J. McCoy, and S. Singer, *J. Chem. Phys.* **85**, 5978 (1986).
- [22] K. Ding, D. Chandler, S. Smithline, and A. Haymet, *Phys. Rev. Lett.* **59**, 1698 (1987).
- [23] J. Lischner and T. Arias, *Phys. Rev. Lett.* **101** (2008).
- [24] W. Kohn and L. Sham, *Phys. Rev.* **140**, A1133 (1965).
- [25] J. Talman and W. Shadwick, *Phys. Rev. A* **14** (1976).
- [26] W. Curtin and N. Ashcroft, *Phys. Rev. A* **32**, 2909 (1985).
- [27] H. Berendsen, J. Grigera, and T. Straatsma, *J. Phys. Chem.* **91** (1987).
- [28] D. Lide, ed., *Handbook of Chemistry and Physics* (CRC Press, Inc., 1995).
- [29] E. Wilhelm, *J. Chem. Phys.* **63** (1975).
- [30] A. Soper, *J. Chem. Phys.* **101** (1994).
- [31] A. Soper, *Chem. Phys.* **258** (2000).
- [32] K. Raghavan, K. Foster, K. Motakabbir, and M. Berkowitz, *J. Chem. Phys.* **94** (1991).
- [33] M. Toney, J. Howard, J. Richer, G. Borges, J. Gordon, O. Melroy, D. Wiesler, D. Yee, and L. Sorensen, *Nature* **368** (1994).
- [34] I.-C. Yeh and M. Berkowitz, *J. Chem. Phys.* **110** (1999).
- [35] X. Xia and M. L. Berkowitz, *Phys. Rev. Lett.* **74**, 3193 (1995).
- [36] F. Booth, *J. Chem. Phys.* **19** (1951).
- [37] G. Sutmann, *J. Electroanal. Chem.* **450** (1998).
- [38] I. Svishchev and P. Kusalik, *J. Phys. Chem.* **98** (1994).
- [39] P. Kusalik and I. Svishchev, *Science* **265** (1994).
- [40] Y. Rosenfeld, *Phys. Rev. Lett.* **63**, 980 (1989).